Research Article Vol. 5, No. 10 / October 2018 / Optica 1247

Origin of the asymmetric light emission from molecular exciton–polaritons

Tomáš Neuman[1] and Javier Aizpurua[1,2,*]

[1]Centro de Física de Materiales de San Sebastián, CFM–MPC (CSIC-UPV/EHU), Paseo Manuel Lardizabal 5, 20018 Donostia-San Sebastián, Spain
[2]Donostia International Physics Center (DIPC), 20018 San Sebastián-Donostia, Spain
*Corresponding author: aizpurua@ehu.eus

Received 23 April 2018; revised 3 September 2018; accepted 5 September 2018 (Doc. ID 330158); published 9 October 2018

Molecular emitters located in an optical cavity are known to experience a dramatic modification of the energy and dynamics of their light emission, establishing novel routes for the generation of non-classical states of light. Under monochromatic illumination, spectral asymmetries in cavity-enhanced molecular fluorescence often emerge due to the formation of hybrid polaritonic states (upper and lower polaritons). By applying the theory of open-quantum systems, we show that under strong-coupling conditions, it is essential to account for the interaction of the molecular electronic states with their vibrational environment (dephasing reservoir) to address the complex dynamics of light emission. The interaction with the dephasing reservoir yields a transfer of energy between the polariton states, favoring the transition toward the lower polariton. As a result, we show that the inelastic light emission originates mainly from the lower polariton state regardless of the pumping laser frequency, thus producing asymmetric light emission spectra. Furthermore, we show that, when several molecules are considered, intermolecular coupling can break the symmetry of the system, enabling originally dark polaritons to emit light, as revealed in the fluorescence spectrum by the emergence of new emission peaks. These results stress that accounting for the interaction with dephasing reservoirs is key to interpret molecular light emission in cavities, consistent with experimental observations.

OCIS codes: (300.6280) Spectroscopy, fluorescence and luminescence; (250.5403) Plasmonics; (270.0270) Quantum optics; (300.6390) Spectroscopy, molecular.

https://doi.org/10.1364/OPTICA.5.001247

1. INTRODUCTION

The interaction of light with molecules has attained much attention due to its potential in the photochemical reactivity of molecules [1], the generation of non-classical states of light [2,3], molecular spectroscopy [4,5], chemical fingerprinting, or in the fundamental investigation of single-molecule properties [2,6–12]. This interaction can be enhanced when a molecule is placed in an optical cavity. To that end, a large variety of optical cavities have been developed, ranging from Fabry–Perot resonators of macroscopic sizes to nanoscale plasmonic cavities where squeezed light is concentrated at (sub)nanometric scales and can interact efficiently with fundamental excitations (e.g., molecular excitons or vibrations) of only a few molecules.

When placed in optical (plasmonic) cavities, excitons in organic molecules can strongly interact with the cavity modes and form new mixed exciton–photon (plasmon) excitations, so-called exciton–polaritons [6,13–42]. Exciton–polaritons have been broadly analyzed in connection with their fluorescence properties, cavity-induced (photo)chemistry [31,32,43–47], polariton lasing and polariton condensation [48–56], and polariton-mediated energy transfer [57,58].

The inelastic photon emission from polariton modes has been found to exhibit spectral asymmetries that favor the emission from the lower polariton branch, while often suppressing the emission from the upper polariton branch [13,30,59–61]. This asymmetry has been attributed to vibrationally driven decay processes between the polaritonic states [62]. It has been shown that the vibrational states of the molecules play a key role in the formation of new vibron–polariton states that lead to the appearance of new peaks in the emission spectra [35,36,38,40,41,63,64]. The excitons in organic molecules are also exposed to interactions with their local environment (the solvent) that produces additional exciton dephasing. The interaction with the solvent molecules also contributes to significant solvent-dependent photoluminescence Stokes shifts induced by the reorganization of the solvent molecules when the solute molecule changes the electronic state [65,66]. It is therefore necessary to correctly treat the interaction of the polariton states with the dephasing reservoir when describing the strong coupling between the cavity mode and the molecular excitons.

In this paper, we address the inelastic light emission spectra of polaritonic systems pumped by a coherent monochromatic laser. We present a quantum-optical model based on the solution of the

quantum master equation [67] that describes the spectral asymmetries observed experimentally in the polariton emission and action (excitation) spectra [13,30,61]. We show that the dominant emission from the lower polariton state is a consequence of the interaction between the excitons and the dephasing reservoir, which in principle includes the effects of both the internal molecular vibrations and the solvent.

2. OPEN QUANTUM SYSTEM THEORY OF (COLLECTIVE) EXCITON-CAVITY-MODE COUPLING

We describe the molecules as two-level electronic systems composed of the ground state, $|g\rangle$, and the excited state, $|e\rangle$, interacting with their respective reservoirs, including both the internal molecular vibrational modes and the fluctuations of the local environment of each molecule [66]. The local environment of a molecule is responsible for the electronic dephasing processes [e.g., vibrations of the molecule or the environment [62,63,68–72], fluctuations of solvent polarization, etc., as presented schematically in Fig. 1(a)]. The two-level excitonic term of the Hamiltonian of the ith molecule is

$$H_{e,i} = \hbar\omega_0 \sigma_i^\dagger \sigma_i, \tag{1}$$

where $\hbar\omega_0$ is the excitonic energy, and σ_i is the two-level-system lowering operator between the many-body excited state, $|e_i\rangle$, and the many-body ground state, $|g_i\rangle$, of the ith molecule, $\sigma_i = |g_i\rangle\langle e_i|$. Each molecule interacts with its local dephasing reservoir described by the Hamiltonian

$$H_{res,i} = \hbar\Omega_R B_i^\dagger B_i, \tag{2}$$

via the exciton–reservoir interaction Hamiltonian

$$H_{e\text{-}res,i} = d_R \Omega_R \sigma_i^\dagger \sigma_i (B_i^\dagger + B_i). \tag{3}$$

Here B_i are the bosonic annihilation operators of the collective reservoir mode i interacting locally with the exciton of the ith molecule [65,70,72–76]. † stands for the Hermitian conjugate. We have assumed that the reservoir modes have the same frequency of $\Omega_{R,e,i} = \Omega_{R,g,i} = \Omega_R$ in the excited state ($\Omega_{R,e,i}$) and the ground state ($\Omega_{R,g,i}$). The equilibrium position of the reservoir mode is rigidly displaced in the electronic excited state of the ith molecule by a dimensionless constant d_R with respect to its equilibrium position in the ground electronic state. As we describe below, we further consider that the reservoir modes are phenomenologically broadened.

The intermolecular excitonic interactions are assumed to be described through the Hamiltonian

$$H_{e\text{-}e} = \sum_{ij} G_{ij} \sigma_i^\dagger \sigma_j + \text{H.c.}, \tag{4}$$

where G_{ij} are coupling constants that generally depend on the spatial distribution of the individual molecules as well as on their mutual orientations.

The molecular excitons interact with a single bosonic cavity mode of frequency ω_c:

$$H_c = \hbar\omega_c a^\dagger a, \tag{5}$$

where $a(a^\dagger)$ is the bosonic annihilation (creation) operator of the cavity mode. The ith molecule interacts with the cavity mode via the coupling Hamiltonian

$$H_{e\text{-}c,i} = \hbar g_i \sigma_i^\dagger a + \text{H.c.}, \tag{6}$$

where g_i is the respective cavity-mode-exciton coupling constant. The total Hamiltonian describing the cavity and molecular excitations finally becomes

$$H_{tot} = H_c + H_{e\text{-}e} + \sum_i (H_{e,i} + H_{res,i} + H_{e\text{-}res,i} + H_{e\text{-}c,i}). \tag{7}$$

The Hamiltonian H_{tot} contains information on the coherent dynamics of the system, but also accounts for the coupling of molecular excitons with their respective dephasing reservoirs. Importantly, H_{tot} does not account for exciton decay and photon leakage. To properly account for this, we describe the dynamics of the system via the master equation for the density matrix, ρ, including the effects of the environment via the phenomenological Lindblad terms of the form $\mathcal{L}_{\mathcal{O}_i}(\rho) = \frac{\gamma_{\mathcal{O}_i}}{2}(2\mathcal{O}_i\rho\mathcal{O}_i^\dagger - \{\mathcal{O}_i^\dagger\mathcal{O}_i, \rho\})$, with $\mathcal{O}_i$ the operator of the respective excitation, the phenomenological damping constants of the respective excitations $\gamma_{\mathcal{O}_i}$, and

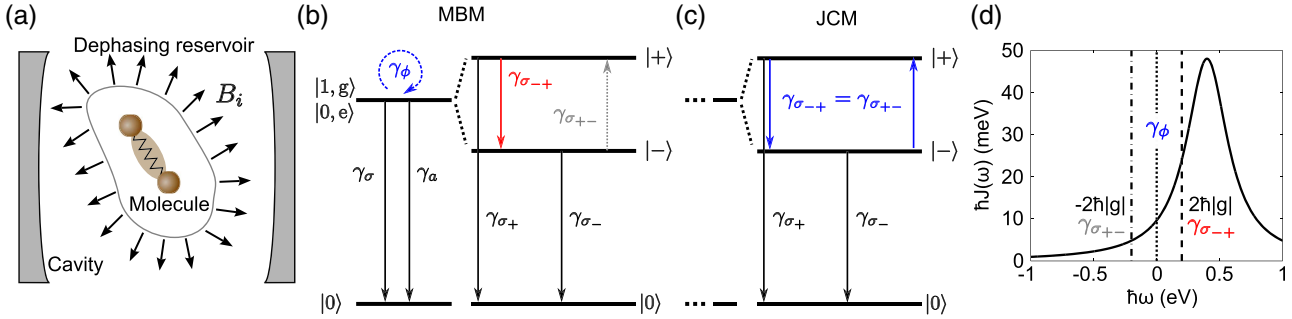

Fig. 1. Effect of dephasing processes on the light emission from a cavity mode strongly coupled with a single exciton. (a) Schematic representation of a molecule interacting with its dephasing bath containing internal molecular vibrations but also environmental degrees of freedom such as fluctuating polarization of the solvent molecules. The bath modes are represented by bosonic annihilation operators B_i. (b) Schematic-level diagrams of an exciton in a cavity that is decoupled (left) and after the coupling is turned on (right) within the MBM. The cavity–exciton coupling gives rise to new polariton states, $|+\rangle$ and $|-\rangle$, and opens new incoherent decay paths between $|+\rangle$ and $|-\rangle$ with respective rates of $\gamma_{\sigma_{-+}} > \gamma_{\sigma_{+-}}$. (c) Level diagram indicating the incoherent population transfer between the polariton states as in panel (b) but for the JCM where the rates $\gamma_{\sigma_{-+}}$ and $\gamma_{\sigma_{+-}}$ are equal ($\gamma_{\sigma_{-+}} = \gamma_{\sigma_{+-}} = \sin^2\theta\cos^2\theta\gamma_\phi$). (d) The bath spectral density $J(\omega)$ is given by Eq. (22) for the parameters $\hbar\gamma_R = 400$ meV, $\hbar\Omega_R = 400$ meV, and $d_R = 0.173$ [for which $\hbar J(0) \approx 20$ meV]. Calculations of selected emission and absorption spectra for smaller values of Ω_R are shown in Supplement 1. The vertical lines indicate the positions where the spectral density is evaluated to obtain the values of the Markovian decay rates $\gamma_{\sigma_{+-}}$, $\gamma_{\sigma_{-+}}$, and γ_ϕ.

with $\{\cdot,\cdot\}$ the anti-commutator. The quantum master equation that includes all the necessary Hamiltonian and Lindblad terms becomes

$$\dot{\rho} = \frac{1}{i\hbar}[H_{\rm tot}, \rho] + \sum_i \mathcal{L}_{\mathcal{O}_i}(\rho), \tag{8}$$

where $\mathcal{O}_i$ depends on the model under consideration. As we detail in what follows, the dynamics encompassed in Eq. (8) leads to the asymmetries observed in the optical response of the strongly coupled system.

3. STRONG COUPLING OF A SINGLE-MOLECULE EXCITON WITH A CAVITY MODE

In the strong-coupling regime, the plasmon–exciton interaction $g_i = g$ becomes so significant that it overcomes the intrinsic electronic ($\gamma_{\sigma_i} = \gamma_\sigma$) and cavity ($\gamma_a$) decay rates and leads to the formation of new hybrid states, polaritonic states. The simplest situation arises when a single cavity mode couples with a single two-level electronic system in the single-excitation manifold, where only the bare states $|{\rm g}, 0\rangle$, $|{\rm e}, 0\rangle$, and $|{\rm g}, 1\rangle$ are considered, with 0 (1) the number of cavity excitations (we omit the index i when talking about a single molecule). The new polaritonic eigenstates $|+\rangle$ and $|-\rangle$ become a coherent admixture of the exciton and the cavity excitation depending on the magnitude of the coupling strength and the detuning of their respective frequencies:

$$\begin{aligned} |+\rangle &= \cos\theta|{\rm e}, 0\rangle + \sin\theta|{\rm g}, 1\rangle, \\ |-\rangle &= -\sin\theta|{\rm e}, 0\rangle + \cos\theta|{\rm g}, 1\rangle, \end{aligned} \tag{9}$$

$$\tan(2\theta) = \frac{2g}{\omega_0 - \omega_{\rm c}} \quad \text{and} \quad 0 < 2\theta < \pi. \tag{10}$$

The scheme of the newly arising energy level structure is drawn schematically in Fig. 1(b) [and 1(c)]. The operators of the three-level system consisting originally of the states $|0\rangle = |{\rm g}, 0\rangle$, $|2\rangle = |{\rm e}, 0\rangle$, and $|3\rangle = |{\rm g}, 1\rangle$ can be more conveniently expressed in the new basis $\{|0\rangle, |+\rangle, |-\rangle\}$ with help of Eq. (9). Most importantly, the operator $\sigma^\dagger\sigma$ responsible for the interaction with the dephasing reservoir in $H_{{\rm e\text{-}res},i} = H_{\rm e\text{-}res}$ becomes (approximated in the single-excitation subspace)

$$\begin{aligned} \sigma^\dagger\sigma \approx |2\rangle\langle 2| &= \cos^2\theta|+\rangle\langle +| + \sin^2\theta|-\rangle\langle -| \\ &\quad - \sin\theta\cos\theta(|-\rangle\langle +| + |+\rangle\langle -|). \end{aligned} \tag{11}$$

We further introduce the simplifying notation $\sigma_{\xi\zeta} = |\xi\rangle\langle\zeta|$, with $\xi, \zeta \in \{+, -\}$ and rewrite the electron-reservoir coupling Hamiltonian as

$$\begin{aligned} H_{\rm e\text{-}res} &= \hbar d_{\rm R}\Omega_{\rm R}\sigma^\dagger\sigma(B^\dagger + B) = \hbar\sigma^\dagger\sigma F \\ &= \hbar[\cos^2\theta\sigma_{++} + \sin^2\theta\sigma_{--} - \sin\theta\cos\theta(\sigma_{-+} + \sigma_{+-})]F, \end{aligned} \tag{12}$$

where we have defined $F = d_{\rm R}\Omega_{\rm R}(B^\dagger + B)$.

Following the standard procedure [67], we now eliminate the dephasing reservoir and derive the incoherent dynamics of the strongly coupled system. To that end, we notice that the operators $\sigma_{+-}, \sigma_{-+}, \sigma_{++}$, and σ_{--} are eigen-operators of the polaritonic Hamiltonian $H_{\rm pol} = H_{\rm c} + H_{\rm e} + H_{\rm e\text{-}c}$ (eigen-operator O of the Hamiltonian $H_{\rm pol}$ defined as $[H_{\rm pol}, O] = \lambda O$, with λ a complex number), and in the interaction picture of $H_{\rm pol}$, these operators have the following time dependences:

$$\sigma_{+-} = \sigma_{+-}^{(0)} e^{-i(\omega_+ - \omega_-)t}, \tag{13}$$

$$\sigma_{-+} = \sigma_{-+}^{(0)} e^{-i(\omega_- - \omega_+)t}, \tag{14}$$

$$\sigma_{++} = \sigma_{++}^{(0)}, \tag{15}$$

$$\sigma_{--} = \sigma_{--}^{(0)}, \tag{16}$$

with $\mathcal{O}^{(0)}$ the Schrödinger-picture operators, and

$$\omega_\pm = \frac{\omega_0 + \omega_{\rm c}}{2} \pm \sqrt{g^2 + \frac{(\omega_0 - \omega_{\rm c})^2}{4}} \tag{17}$$

the frequencies of the upper (ω_+) and lower (ω_-) polaritons.

In the secular approximation, the incoherent processes are represented by the Lindblad terms describing the dephasing of the polariton states, $\mathcal{L}_{\sigma_{++--}}(\rho)$, the decay of $|+\rangle$ to $|-\rangle$, $\mathcal{L}_{\sigma_{-+}}(\rho)$, and the reverse process, $\mathcal{L}_{\sigma_{+-}}(\rho)$. For brevity, we have defined $\sigma_{++--} = \cos^2\theta\sigma_{++} + \sin^2\theta\sigma_{--}$. The respective dephasing and decay rates, $\gamma_\phi = \gamma_{\sigma_{++--}}$, $\gamma_{\sigma_{-+}}$, and $\gamma_{\sigma_{+-}}$, are determined from the properties of the dephasing reservoir characterized by its spectral density $J(\omega)$:

$$\gamma_{\sigma_{-+}} = \cos^2\theta\sin^2\theta J(\omega_+ - \omega_-), \tag{18}$$

$$\gamma_{\sigma_{+-}} = \cos^2\theta\sin^2\theta J(\omega_- - \omega_+), \tag{19}$$

$$\gamma_\phi = J(0). \tag{20}$$

The spectral density of the reservoir [65,70,72,74–76] is obtained as the Fourier transform of the reservoir's two-time correlation function $\langle F^\dagger(t+s)F(t)\rangle$ [67]:

$$J(\omega) = 2\Re\left\{\int_0^\infty {\rm d}s e^{i\omega s}\langle F^\dagger(t+s)F(t)\rangle\right\}, \tag{21}$$

where $\Re\{\cdot\}$ is the real part. In particular, $J(\omega)$ emerging from Eqs. (2) and (3) together with the Lindblad term $\mathcal{L}_{B_i}(\rho) = \mathcal{L}_B(\rho)$ (damped harmonic-oscillator reservoir [65,75]) calculated for zero temperature, $T = 0$ K, is

$$J(\omega) = \frac{2\gamma_B d_{\rm R}^2\Omega_{\rm R}^2}{(\Omega_{\rm R} - \omega)^2 + \gamma_B^2}. \tag{22}$$

The spectral density, $J(\omega)$, of the considered vibrational bath [Eq. (22)] is shown in Fig. 1(d). $J(\omega)$ has the form of a broad Lorentzian peak positioned at the positive side of the frequency axis. This stems from the condition $T = 0$ K, for which the polariton decay can result only in the spontaneous generation of excitations (vibrations) in an otherwise unpopulated reservoir. We note that for $T > 0$ K (a situation not considered in this paper), when the reservoir acquires thermal population, processes including absorption of a thermal reservoir excitation (appearing for negative ω) would also contribute to $J(\omega)$ [72,77–80]. The model parameters used in our study are specified in the caption of Fig. 1. As $J(\omega)$ is not symmetrical with respect to the zero frequency, the transition $|+\rangle \to |-\rangle$ given by the rate $\gamma_{\sigma_{-+}} = \cos^2\theta\sin^2\theta J(2|g|)$ is favored compared with the $|-\rangle \to |+\rangle$ transition occurring with a rate of $\gamma_{\sigma_{+-}} = \cos^2\theta\sin^2\theta J(-2|g|)$ [indicated by vertical lines in Fig. 1(d)]. We stress that this asymmetry is a general property of dephasing reservoirs and robustly appears in a wide range of non-Markovian dephasing models [70,73,74,76]. This imbalance of transfer of energy between the polariton states gives rise to the asymmetries observed in the emission spectra [13,30,61] that we address below.

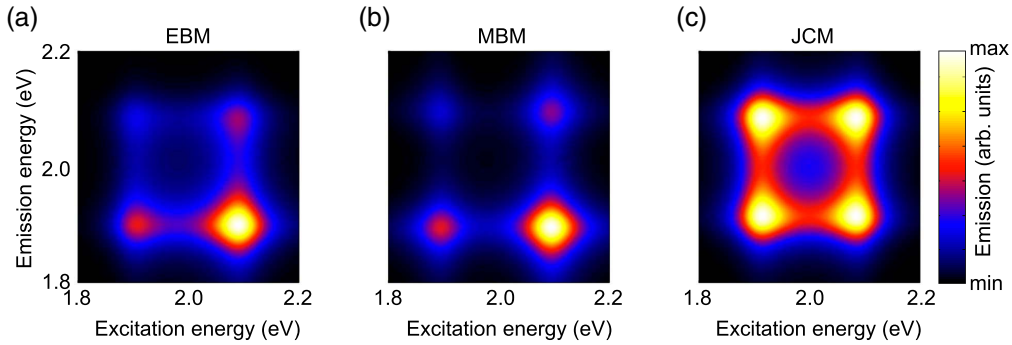

Fig. 2. Photon emission spectra normalized to the incident laser intensity $|\mathcal{E}|^2$ as a function of excitation frequency $\omega_{\rm L}$ within (a) the explicit-bath model, (b) the Markovian-bath model, and (c) the Jaynes–Cummings model. In all the calculations, we have considered the parameters $\hbar\omega_0 = \hbar\omega_{\rm c} = 2$ eV, $\hbar\gamma_a = 150$ meV, $\hbar\gamma_\sigma = 2\times10^{-2}$ meV, and $\hbar g = 100$ meV. The pure dephasing constant for JCM is $\gamma_\phi = J(0)$. The parameters of the bath are $\hbar\gamma_B = 400$ meV, $\hbar\Omega_{\rm R} = 400$ meV, and $d_{\rm R} = 0.173$.

Last, in strong coupling, we employ the polariton Lindblad operators $\mathcal{L}_{\sigma_+}(\rho)$ and $\mathcal{L}_{\sigma_-}(\rho)$ ($\sigma_+ = |0\rangle\langle+|$ and $\sigma_- = |0\rangle\langle-|$), where the decay rates of the upper, γ_{σ_+}, and the lower, γ_{σ_-}, polaritons are defined, respectively, as

$$\gamma_{\sigma_+} = \gamma_a \sin^2\theta, \tag{23}$$

$$\gamma_{\sigma_-} = \gamma_a \cos^2\theta, \tag{24}$$

where γ_a is the decay rate of the bare cavity decoupled from the molecules. The phenomenological Lindblad terms $\mathcal{L}_{\sigma_+}(\rho)$ and $\mathcal{L}_{\sigma_-}(\rho)$ can be related to the commonly assumed phenomenological Lindblad super-operator describing the decay of the bare cavity, $\mathcal{L}_a(\rho)$. Under the strong-coupling condition, we write the photon annihilation operator a in terms of the polariton operators σ_+ and σ_- (in the single-excitation subspace):

$$a \approx \sin\theta\sigma_+ + \cos\theta\sigma_-, \tag{25}$$

and apply the secular approximation. Under such conditions, the Lindblad super-operator $\mathcal{L}_a(\rho)$ approximately transforms into a pair of the Lindblad terms, $\mathcal{L}_{\sigma_+}(\rho)$ and $\mathcal{L}_{\sigma_-}(\rho)$:

$$\mathcal{L}_a(\rho) \approx \mathcal{L}_{\sigma_+}(\rho) + \mathcal{L}_{\sigma_-}(\rho). \tag{26}$$

We also phenomenologically include the intrinsic molecular losses via $\mathcal{L}_\sigma(\rho)$, considering $\gamma_\sigma \ll \gamma_a$.

4. POLARITON EMISSION SPECTRA UNDER COHERENT DRIVING CONDITIONS

A. Single Molecule in a Cavity

In what follows, we consider several different approaches to the implementation of dephasing due to the reservoir. First, we explicitly implement the dephasing reservoir defined by $H_{{\rm res},i} = H_{\rm res}$ and $H_{{\rm e\text{-}res},i} = H_{\rm e\text{-}res}$ [Eqs. (2) and (3), respectively] and $\mathcal{L}_B(\rho)$ into the master equation as part of the simulated system [the explicit-bath model (EBM)] and solve for the spectral response (see Supplement 1 for details of the implementation of the reservoir degrees of freedom). In the second approach, we approximate the EBM and eliminate the dephasing reservoir from Eq. (8) using the Born–Markov and secular approximations, as described in the previous section, and introduce the effective dephasing and damping terms via the Lindblad super-operators $\mathcal{L}_\sigma(\rho)$, $\mathcal{L}_{\sigma_+}(\rho)$, $\mathcal{L}_{\sigma_-}(\rho)$, $\mathcal{L}_{\sigma_{++--}}(\rho)$, $\mathcal{L}_{\sigma_{-+}}(\rho)$, and $\mathcal{L}_{\sigma_{+-}}(\rho)$ [the Markovian-bath model (MBM)]. The effective rates are depicted schematically in Fig. 1(b).

As a third approach, we consider the commonly adopted Jaynes–Cummings model (JCM) where the effective dephasing and decay rates are first defined for the exciton of the molecule and the bare cavity mode, which are mutually decoupled. Note that this is in contrast with the MBM where the incoherent dynamics is derived in the polariton basis. The decays of the cavity and the molecular exciton are described in the JCM by $\mathcal{L}_a(\rho)$ and $\mathcal{L}_\sigma(\rho)$, respectively, as defined earlier, and the pure dephasing is implemented via

$$\mathcal{L}_{\sigma^\dagger\sigma}(\rho) = \frac{\gamma_\phi}{2}(2\sigma^\dagger\sigma\rho\sigma^\dagger\sigma - \{\sigma^\dagger\sigma,\rho\}). \tag{27}$$

In the JCM, the interaction with the reservoir given in Eqs. (2) and (3) is not considered. Upon transformation into the polariton basis, the dephasing term in the JCM yields (among others) the interaction terms between $|+\rangle$ and $|-\rangle$, with equal rates for the $|+\rangle \to |-\rangle$ and $|-\rangle \to |+\rangle$ transitions, as depicted schematically in Fig. 1(c).

As we are interested in the response of the system under illumination by a monochromatic laser light, we introduce the driving term

$$H_{\rm pump} = \mathcal{E}(a^\dagger e^{-i\omega_{\rm L}t} + a e^{i\omega_{\rm L}t}), \tag{28}$$

where $\mathcal{E}$ is the amplitude of the laser pumping and $\omega_{\rm L}$ is the laser frequency. We make sure that the pumping amplitude is small enough to conform with the single-excitation approximation.

We calculate the absorption spectra, $s_{\rm A}(\omega)$, of the system (assuming only the cavity interacts with the radiation field) and the inelastic emission spectra, $s_{\rm E}(\omega;\omega_{\rm L})$, for different frequencies $\omega_{\rm L}$ of the incident pumping laser. The spectra are calculated from the quantum regression theorem as one-sided Fourier transforms of the two-time correlation functions (more details are provided in Supplement 1):

$$s_{\rm A}(\omega) = 2\Re\int_0^\infty \langle\langle a(\tau)a^\dagger(0)\rangle\rangle_{\rm ss} e^{i\omega\tau}{\rm d}\tau, \tag{29}$$

$$s_{\rm E}(\omega;\omega_{\rm L}) = 2\Re\int_0^\infty \langle\langle a^\dagger(\tau)a(0)\rangle\rangle_{\rm ss} e^{-i\omega\tau}{\rm d}\tau, \tag{30}$$

where the double-angle brackets are defined as $\langle\langle a^\dagger(\tau)a(0)\rangle\rangle_{\rm ss} = \langle a^\dagger(\tau)a(0)\rangle_{\rm ss} - \lim_{\tau\to\infty}\langle a^\dagger(\tau)a(0)\rangle_{\rm ss}$.

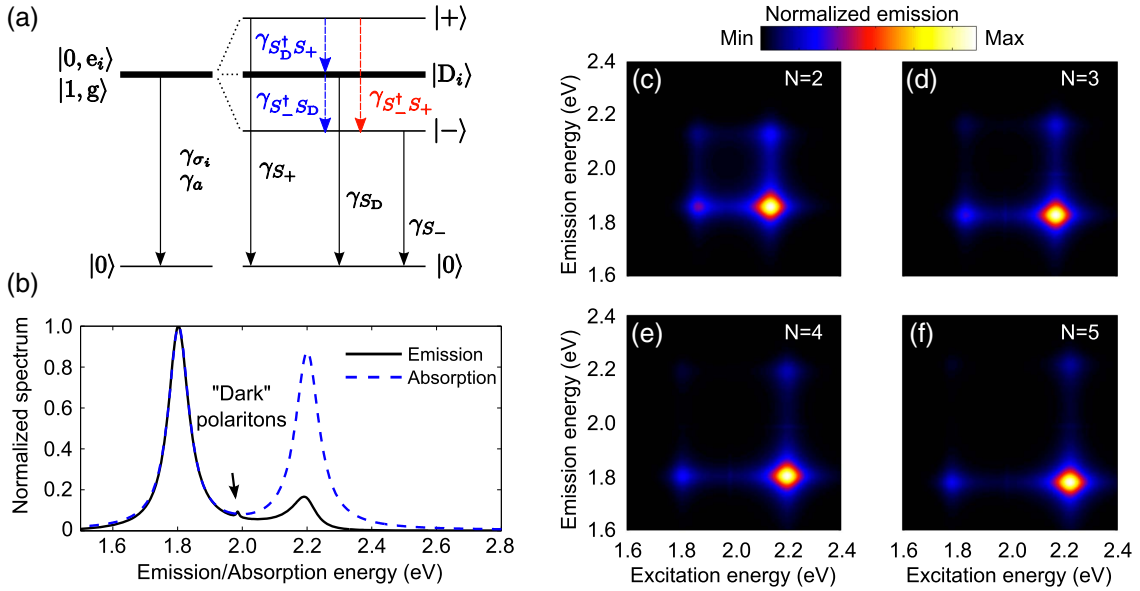

Fig. 3. (a) Schematic representation of the polariton incoherent dynamics obtained from the full model. The strong coupling leads to formation of bright upper, $|+\rangle$, and lower, $|-\rangle$, polaritons that are decoupled from the dark states, $|\mathrm{D}_i\rangle$. The coupling of the polariton and the dark states with the dephasing reservoir gives rise to the incoherent transfer of populations from the higher energy states to the lower energy states. The bare cavity incoherently decays with rate γ_a, the excitons of the bare molecules incoherently decay with rates $\gamma_{\sigma_i} = \gamma_\sigma$. The bright polariton states $|+\rangle$ and $|-\rangle$ then experience the incoherent decay into the ground state $|0\rangle$ with rates γ_{S_+} and γ_{S_-}, respectively. The dark polaritons decay to the ground state with equal rates $\gamma_{S_\mathrm{D}} = \gamma_\sigma$. Finally, population transfer among the polariton branches occurs with rates $\gamma_{S_{\mathrm{D}_i}^\dagger S_+}$, $\gamma_{S_-^\dagger S_\mathrm{D}}$, and $\gamma_{S_-^\dagger S_+}$, as marked in the schematic. The population transfer is accompanied by dephasing processes (not shown). (b) Emission (black line) and absorption (blue dashed line) spectra of four molecular excitons ($N = 4$) coupled to the cavity mode. The emission from $|-\rangle$ prevails over the $|+\rangle$ emission due to the incoherent population transfer caused by the dephasing reservoir. The absorption spectrum, on the other hand, contains both $|+\rangle$ and $|-\rangle$ peaks of similar intensity. Last, the emission and absorption spectra each contain a peak appearing close to the frequency of the decoupled molecules that arises from the dark polariton states $|\mathrm{D}_i\rangle$ that are now coupled to the bright polaritons $|+\rangle$ and $|-\rangle$. [(c)–(f)] Emission spectra as a function of excitation energy $\hbar\omega_\mathrm{L}$ for $N = 2, 3, 4, 5$ molecules, respectively. In all the cases, (b)–(f) show that the molecular excitons of equal energies $\hbar\omega_0 = 2$ eV are perfectly tuned to the cavity resonance $\hbar\omega_\mathrm{c} = 2$ eV and interact with the cavity mode via $\hbar g_i = \hbar g = 100$ meV. The system is pumped by a laser of amplitude $\hbar\mathcal{E} = 0.1$ meV. Additional parameters are $\hbar\gamma_a = 150$ meV, $\hbar\gamma_B = 400$ meV, $\hbar\gamma_\sigma = 2 \times 10^{-2}$ meV, $d = 0.173$, and $\hbar\Omega_\mathrm{R} = 400$ meV.

The calculated emission spectra for the reservoir spectral density assumed in Fig. 1(d) are shown in Fig. 2 within both the EBM and MBM, and are compared with the result obtained from the JCM. To simplify the discussion, in what follows we concentrate on the special case when the energies of the plasmonic and excitonic transitions are matched ($\omega_\mathrm{c} = \omega_0$). In Figs. 2(a)–2(c), we plot the emission spectra of the strongly coupled single-molecule exciton with the cavity mode as a function of excitation frequency ω_L within (a) the EBM, (b) the MBM, and (c) the JCM. For both the EBM and MBM, the color maps offer the same qualitative and very similar quantitative results. The inelastic emission arises mainly from the transition of the lower polariton to the ground state and thus leads to a clear dominance of the emission peak of the lower polariton. Contrarily, the JCM yields a fully symmetrical result independently of the excitation frequency, which contradicts the experimental evidence [13,30,61]. The implementation of the dephasing in the JCM is thus unable to correctly describe the imbalance in the dephasing-driven population transfer between the polaritonic states.

B. Many Molecules in a Cavity

The strong coupling between a single-molecule exciton and a cavity mode is fundamentally important; however, in realistic systems, the cavity is usually coupled to several molecular samples [81]. We therefore extend our description to cavities containing N molecules and calculate the absorption and emission spectra as defined in Eqs. (29) and (30), respectively, using the EBM. In the EBM, we include the Lindblad terms $\mathcal{L}_{B_i}(\rho)$, $\mathcal{L}_{\sigma_i}(\rho)$, $\mathcal{L}_{S_+}(\rho)$, and $\mathcal{L}_{S_-}(\rho)$, where $S_+ = |0\rangle\langle+|$ and $S_- = |0\rangle\langle-|$ [with $|0\rangle$ the ground state and $|+\rangle$ ($|-\rangle$) the upper (lower) polariton branches]. We consider $\gamma_{\sigma_i} = \gamma_\sigma$ and $\gamma_{B_i} = \gamma_B$. More details are provided in Supplement 1. Like in the single-molecule case, the strong coupling of the cavity mode with the excitons of many molecules gives rise to the upper ($|+\rangle$) and lower ($|-\rangle$) polariton branches, as depicted schematically in Fig. 3(a). In addition to the bright polaritons $|+\rangle$ and $|-\rangle$, there are $N - 1$ states that are decoupled from the cavity [if the intermolecular interaction in Eq. (4) preserves the equivalence of all the molecules] and are commonly called *dark* polaritons $|\mathrm{D}_i\rangle$. The polariton states incoherently couple via the dephasing reservoir, which allows population transfer among the bright polaritons ($|+\rangle$ and $|-\rangle$) and the dark $|\mathrm{D}_i\rangle$ polaritons $\gamma_{S_{\mathrm{D}_i}^\dagger S_+} = \gamma_{S_\mathrm{D}^\dagger S_+}$, $\gamma_{S_{\mathrm{D}_i}^\dagger S_-} = \gamma_{S_\mathrm{D}^\dagger S_+}$, and $\gamma_{S_-^\dagger S_+}$, with decay rates of $\gamma_{\sigma_i} = \gamma_{S_{\mathrm{D}_i}} = \gamma_{S_\mathrm{D}} = \gamma_\sigma$ for the dark polaritons, and γ_{S_+} and γ_{S_-} for the bright polaritons. The incoherent processes can be included into the system dynamics via the Lindblad terms $\mathcal{L}_{\mathcal{O}_i}(\rho)$, with the respective rates of $\gamma_{\mathcal{O}_i}$, and $\mathcal{O}_i \in \{S_{\mathrm{D}_i}^\dagger S_+, S_-^\dagger S_{\mathrm{D}_i}, S_-^\dagger S_+, S_{\mathrm{D}_i}, S_+, S_-\}$. In our notation, $S_\xi = |0\rangle\langle\xi|$ (with $|0\rangle$ the ground state). The newly arising states also undergo dephasing (not shown in the schematics), in analogy with the case of the single exciton. More details on the respective processes are provided in Supplement 1. As opposed to the case where only a

single molecule is considered, in the collective scenario, the dark polariton states mediate the population decay $|+\rangle \rightarrow |-\rangle$ and change the population dynamics observed for the lower polariton state if $|+\rangle$ is pumped.

In the following, we assume an intermolecular coupling of the form

$$G_{ij} = \frac{G_0}{|i-j|^3} \quad \text{for } i \neq j \quad \text{and}$$
$$G_{ij} = 0 \quad \text{for } i = j, \tag{31}$$

and set

$$\hbar G_0 = \frac{p_0^2}{4\pi\varepsilon_0 r_0^3}, \tag{32}$$

with $p_0 = 0.2\ \mathrm{e}\cdot\mathrm{nm}$ the transition dipole moment of the exciton; $r_0 = 2$ nm the effective intermolecular distance; and ε_0 the vacuum permittivity. This choice of G_{ij} describes a set of interacting molecules whose dipoles are arranged along a line (e.g., in x direction) with a constant spacing of r_0 and with parallel dipole moments p_0 (e.g., oriented along z). The intermolecular interaction given by Eq. (31) weakly perturbs the polariton structure given by the collective cavity-mode-exciton Hamiltonian; however, it breaks the symmetry of the Hamiltonian (makes the molecules inequivalent). Due to this symmetry breaking, the originally dark polariton states $|\mathrm{D}_i\rangle$ couple with the cavity mode and become observable in the spectra. We discuss more details of the collective-coupling model in Supplement 1. We note that the symmetry of the system Hamiltonian can be broken in different ways, for example, by introducing disorder into the system.

As an illustrative example, we calculate the emission and absorption spectra of four mutually interacting molecules that are coupled to the cavity with $\hbar g_i = \hbar g = 100$ meV. The system is pumped at an upper polariton frequency of $\hbar\omega_{\mathrm{L}} = 2.2$ eV. The result is shown in Fig. 3(b) for $N = 4$ molecules interacting with the cavity mode. The emission spectrum (black solid line) shows a dominant peak originating from the lower polariton $|-\rangle$ (appearing at ≈1.8 eV) as in the single-molecular case. Another sharp emission peak of low intensity, which was not present in the single-molecule case, emerges at a frequency around that of the decoupled molecules, i.e., ≈2 eV. This new peak is a signature of the polariton states $|\mathrm{D}_i\rangle$ that are dark in the collective-coupling model where the excitons do not interact directly among themselves, but become bright after introducing the intermolecular coupling in Eq. (4). Experiments where large numbers of molecules couple with the cavity show that the photoluminescence peak of the dark polariton can have comparable intensity to the emission peaks of the lower polaritons [30,61]. On the other hand, the absorption spectrum (blue dashed line) features two absorption peaks of commensurate intensity at the frequencies of the $|+\rangle$ and $|-\rangle$ polariton branches. As a result of the inter-polariton transfer induced by the reservoir, the lower-polariton peak has slightly higher spectral intensity and is narrower than the upper-polariton peak, since the latter is broadened by the decay processes induced by the dephasing reservoir [72].

Finally, in Figs. 3(c)–3(f) we present two-dimensional maps containing the emission (vertical axis) and excitation (horizontal axis) spectra of systems containing $N = 2$ [Fig. 3(c)], $N = 3$ [Fig. 3(d)], $N = 4$ [Fig. 3(e)], and $N = 5$ [Fig. 3(f)] molecules (considering $\hbar g = 100$ meV). The emission pattern is in all the cases similar to that in the single-molecule case [Figs. 2(a) and 2(b)], exhibiting a doublet of emission peaks originating from $|+\rangle$ and $|-\rangle$ that are split by the collectively enhanced coupling $\sqrt{N}g$. Between the $|+\rangle$ and $|-\rangle$ polariton peaks, in this collective scenario, there appears an additional feature corresponding to the dark polaritons in both the emission and excitation spectra, which is hardly distinguishable in the spectral maps. The dominance of the lower-polariton peak in all calculated spectra is in accordance with the mechanism of incoherent population transfer in strongly coupled systems discussed above. We can observe that the inelastic emission from the lower polariton branch is the most efficient when the upper polariton is pumped. In this case, the interaction with the reservoir efficiently incoherently populates $|-\rangle$, which in turn emits the inelastic photons. We now briefly analyze the polariton dynamics in the collective scenario that gives rise to the asymmetry of the inelastic photon emission.

5. POLARITON DYNAMICS IN THE COLLECTIVE SCENARIO

We have shown that the dephasing reservoir gives rise to incoherent transitions between the polariton states that preferentially lead from the states of higher energy toward the states of lower energy ($|+\rangle \rightarrow |\mathrm{D}_i\rangle$, $|+\rangle \rightarrow |-\rangle$, and $|\mathrm{D}_i\rangle \rightarrow |-\rangle$). This phenomenology has been addressed in detail by other authors [72,77–80]. Here we briefly complete the discussion of our model and focus on the dynamics of these decay processes, and calculate the time evolution of the polariton populations $n_+ = \langle S_+^\dagger S_+\rangle$, $n_- = \langle S_-^\dagger S_-\rangle$, and $n_{\mathrm{D}} = \frac{1}{N-1}\sum_i \langle S_{\mathrm{D}_i}^\dagger S_{\mathrm{D}_i}\rangle$ assuming that the populations evolve according to the master equation [Eq. (8) with Eq. (26)] that explicitly includes the dephasing reservoir (the EBM). We compare the EBM population dynamics with the dynamics of a rate-equation model (REM) based on the diagram of levels and decays displayed in Fig. 3(a) (more details are provided in Supplement 1). In the REM, only the incoherent dynamics of the populations of the respective states is studied (the population decay) and processes related with pure dephasing are not considered. We calculate the dynamics assuming the upper polariton is initially fully populated, $n_+ = 1$ and $n_- = n_{\mathrm{D}} = 0$, and then decays spontaneously (the coherent driving [Eq. (28)] is switched off) to the ground state $|0\rangle$ and to the other polariton states, namely, $|-\rangle$ and $|\mathrm{D}_i\rangle$.

In Fig. 4, we plot the polariton populations on a logarithmic scale as a function of time obtained from the numerical time evolution of the full system-reservoir density matrix (EBM—dashed lines) together with the solution of the REM (full lines) for $N = 4$ molecules [Fig. 4(a)] and $N = 1000$ molecules [Fig. 4(b)] (using the REM only). For $N = 4$, the REM matches well with the EBM, with only slight deviations from the exact population dynamics. n_+ (black) exhibits a rapid decay at a total rate of γ_{n_+} [$\gamma_{n_+} = \gamma_{S_+} + \gamma_{S_-^\dagger S_+} + (N-1)\gamma_{S_{\mathrm{D}}^\dagger S_+}$] from its original population to the ground state, $|0\rangle$ (γ_{S_+}), but also to the lower polariton, $|-\rangle$ ($\gamma_{S_-^\dagger S_+}$), and the dark polaritons, $|\mathrm{D}_i\rangle$, at a rate of $(N-1)\gamma_{S_{\mathrm{D}}^\dagger S_+}$ that pumps the lower (n_-, red) and dark polariton (n_{D}, blue) populations. After this initial impulse, the dark polariton population starts to steadily decay to the ground state ($\gamma_{S_{\mathrm{D}}}$) and to the lower-polariton state ($\gamma_{S_-^\dagger S_{\mathrm{D}}}$). Similarly to the dark polaritons, the lower polariton first gets populated due to the fast-decaying upper polariton. After that, $|-\rangle$ rapidly decays to the ground state (γ_{S_-}), but only until it reaches the regime when

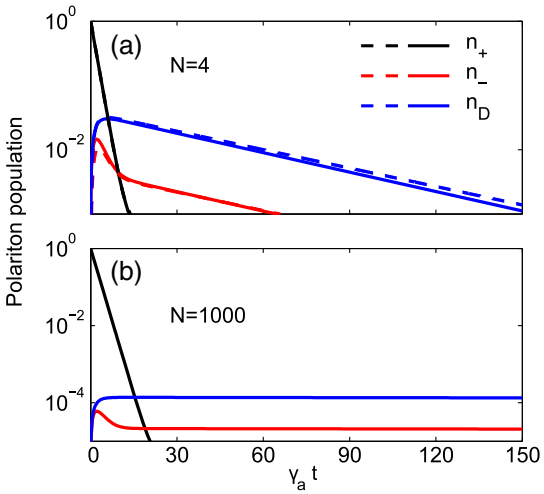

Fig. 4. Decay of polariton populations, n_+ (upper polariton—black), n_- (lower polariton—red), and n_D (dark polariton—blue), on a logarithmic scale as a function of time assuming that initially $n_+ = 1$ and $n_- = n_D = 0$. (a) The full calculation (EBM—dashed lines) is compared with the REM (full lines) for $N = 4$ molecules and $g = 100$ meV. (b) The populations calculated from the REM for $N = 1000$ molecules, using $\sqrt{N}g = 200$ meV. The remaining parameters are $\hbar\gamma_a = 150$ meV, $\hbar\gamma_B = 400$ meV, $\hbar\gamma_\sigma = 2 \times 10^{-2}$ meV, $d = 0.173$, and $\hbar\Omega_R = 400$ meV.

n_- is dominantly pumped by the slowly decaying dark polariton ($\gamma_{S_-^\dagger S_D}$). In this regime, the decay of n_- becomes limited by the pumping and resembles that of the dark polaritons [the *bottleneck* effect; red lines in Fig. 4(a)].

In Supplement 1, we show that the decay rates connecting the polariton states are inversely proportional to the number of molecules, $\gamma_{S_+^\dagger S_-}, \gamma_{S_-^\dagger S_+}, \gamma_{S_-^\dagger S_D}, \gamma_{S_D^\dagger S_-}, \gamma_{S_+^\dagger S_D}, \gamma_{S_D^\dagger S_+} \propto 1/N$. Since the upper and lower polaritons in our model decay fast to the ground state ($\gamma_{S_+}, \gamma_{S_-} \propto \gamma_a$) regardless of N, the initial stages of their respective population dynamics are practically independent of the number of molecules. However, as N is increased, the rate of decay of the dark polariton to the lower polariton becomes progressively smaller ($\gamma_{S_-^\dagger S_D} \propto 1/N$) until it becomes fully limited by the intrinsic rate γ_σ for $N \to \infty$. This tendency is apparent from Fig. 4(b) where we plot the population decay for $N = 1000$ molecules as obtained from the REM.

Finally, we remark that the model described in this paper is capable of addressing the dynamics of population transfer among polaritonic states, but does not explain the long lifetime of the lower polariton state that has been reported in the literature [62,82–84]. In our approach, the terminal slow decay of n_- arises due to a *bottleneck* in the form of a slowly decaying *dark* polariton state. The explanation of the long lower-polariton lifetime requires further modeling of the microscopic decay mechanisms of the coupled cavity mode and the molecular excitons.

6. CONCLUSION

In conclusion, we have demonstrated that the dephasing reservoir in strongly coupled cavity-mode-exciton systems can lead to asymmetries in the observed emission spectra, favoring the light emission from the lower polariton and suppressing the emission from the upper polariton. The asymmetry in the inelastic light emission from the cavity arises naturally from the model, which explicitly considers the dephasing bath as an effective damped-harmonic oscillator. The coupling with the reservoir in the strong-coupling regime naturally favors the transfer of the population of higher-energy polaritons toward the polaritons of lower energy ($|+\rangle \to |D_i\rangle$, $|+\rangle \to |-\rangle$, and $|D_i\rangle \to |-\rangle$), including the dark polaritons if many molecules are considered. This process leads to the prevalence of the inelastic photon emission from the lower polariton $|-\rangle$ and a considerably shorter lifetime of the upper polariton $|+\rangle$. Moreover, if many mutually interacting molecules are coupled to the cavity, the dark polariton states can become bright and give rise to a new peak in the polariton emission spectrum. This new peak is then positioned approximately at the frequency of the uncoupled excitons, which is consistent with the experimental observations [13,30,61].

The results presented in this paper provide an intuitive view of the processes that stand behind the experimental observations and can serve as guidelines for future implementations of dephasing in strongly coupled systems.

Funding. Spanish Ministry of Science, Innovation and Universities (MICIN) (FIS2016-80174-P); Physical Measurement Laboratory (PML) of NIST (70NANB15H32); Department of Education of the Basque Government (IT-756-13).

Acknowledgment. We acknowledge Prof. Thomas Ebbesen from University of Strasbourg for inspiring discussions.

See Supplement 1 for supporting content.

REFERENCES

1. M. Klessinger and J. Michl, *Excited States and Photochemistry of Organic Molecules* (Wiley, 1995).
2. S. Kühn, U. Håkanson, L. Rogobete, and V. Sandoghdar, "Enhancement of single-molecule fluorescence using a gold nanoparticle as an optical nanoantenna," Phys. Rev. Lett. **97**, 017402 (2006).
3. G. M. Akselrod, C. Argyropoulos, T. B. Hoang, C. Ciracì, C. Fang, J. Huang, D. R. Smith, and M. H. Mikkelsen, "Probing the mechanisms of large Purcell enhancement in plasmonic nanoantennas," Nat. Photonics **8**, 835–840 (2014).
4. R. F. Aroca, "Plasmon enhanced spectroscopy," Phys. Chem. Chem. Phys. **15**, 5355–5363 (2013).
5. T. Itoh, Y. S. Yamamoto, and Y. Ozaki, "Plasmon-enhanced spectroscopy of absorption and spontaneous emissions explained using cavity quantum optics," Chem. Soc. Rev. **46**, 3904–3921 (2017).
6. D. G. Lidzey, D. Bradley, M. Skolnick, T. Virgili, S. Walker, and D. Whittaker, "Strong exciton–photon coupling in an organic semiconductor microcavity," Nature **395**, 53–55 (1998).
7. B. Doppagne, M. C. Chong, E. Lorchat, S. Berciaud, M. Romeo, H. Bulou, A. Boeglin, F. Scheurer, and G. Schull, "Vibronic spectroscopy with submolecular resolution from STM-induced electroluminescence," Phys. Rev. Lett. **118**, 127401 (2017).
8. L. Zhang, Y.-J. Yu, L.-G. Chen, Y. Luo, B. Yang, F.-F. Kong, G. Chen, Y. Zhang, Q. Zhang, Y. Luo, J. L. Yang, Z.-C. Dong, and J. G. Hou, "Electrically driven single-photon emission from an isolated single molecule," Nat. Commun. **8**, 580 (2017).
9. Y. Zhang, Q.-S. Meng, L. Zhang, Y. Luo, Y.-J. Yu, B. Yang, Y. Zhang, R. Esteban, J. Aizpurua, Y. Luo, J. L. Yang, Z.-C. Dong, and J. G. Hou, "Sub-nanometre control of the coherent interaction between a single molecule and a plasmonic nanocavity," Nat. Commun. **8**, 15225 (2017).
10. H. Imada, K. Miwa, M. Imai-Imada, S. Kawahara, K. Kimura, and Y. Kim, "Single-molecule investigation of energy dynamics in a coupled plasmon–exciton system," Phys. Rev. Lett. **119**, 013901 (2017).
11. F. Benz, M. K. Schmidt, A. Dreismann, R. Chikkaraddy, Y. Zhang, A. Demetriadou, C. Carnegie, H. Ohadi, B. de Nijs, R. Esteban,

J. Aizpurua, and J. J. Baumberg, "Single-molecule optomechanics in 'picocavities'," Science **354**, 726–729 (2016).
12. G. Wrigge, I. Gerhardt, J. Hwang, G. Zumofen, and V. Sandoghdar, "Efficient coupling of photons to a single molecule and the observation of its resonance fluorescence," Nat. Phys. **4**, 60–66 (2008).
13. P. A. Hobson, W. L. Barnes, D. G. Lidzey, G. A. Gehring, D. M. Whittaker, M. S. Skolnick, and S. Walker, "Strong exciton–photon coupling in a low-Q all-metal mirror microcavity," Appl. Phys. Lett. **81**, 3519–3521 (2002).
14. J. Bellessa, C. Bonnand, J. C. Plenet, and J. Mugnier, "Strong coupling between surface plasmons and excitons in an organic semiconductor," Phys. Rev. Lett. **93**, 036404 (2004).
15. J. Dintinger, S. Klein, F. Bustos, W. L. Barnes, and T. W. Ebbesen, "Strong coupling between surface plasmon–polaritons and organic molecules in subwavelength hole arrays," Phys. Rev. B **71**, 035424 (2005).
16. P. Michetti and G. C. La Rocca, "Polariton states in disordered organic microcavities," Phys. Rev. B **71**, 115320 (2005).
17. A. Trügler and U. Hohenester, "Strong coupling between a metallic nanoparticle and a single molecule," Phys. Rev. B **77**, 115403 (2008).
18. T. Schwartz, J. A. Hutchison, C. Genet, and T. W. Ebbesen, "Reversible switching of ultrastrong light-molecule coupling," Phys. Rev. Lett. **106**, 196405 (2011).
19. D. M. Coles, P. Michetti, C. Clark, W. C. Tsoi, A. M. Adawi, J.-S. Kim, and D. G. Lidzey, "Vibrationally assisted polariton-relaxation processes in strongly coupled organic-semiconductor microcavities," Adv. Funct. Mater. **21**, 3691–3696 (2011).
20. V. Agranovich, Y. N. Gartstein, and M. Litinskaya, "Hybrid resonant organic–inorganic nanostructures for optoelectronic applications," Chem. Rev. **111**, 5179–5214 (2011).
21. A. Salomon, R. J. Gordon, Y. Prior, T. Seideman, and M. Sukharev, "Strong coupling between molecular excited states and surface plasmon modes of a slit array in a thin metal film," Phys. Rev. Lett. **109**, 073002 (2012).
22. S. Kéa-Cohen, S. A. Maier, and D. D. C. Bradley, "Ultrastrongly coupled exciton–polaritons in metal-clad organic semiconductor microcavities," Adv. Opt. Mater. **1**, 827–833 (2013).
23. P. Vasa, W. Wang, R. Pomraenke, M. Lammers, M. Maiuri, C. Manzoni, G. Cerullo, and C. Lienau, "Real-time observation of ultrafast Rabi oscillations between excitons and plasmons in metal nanostructures with J-aggregates," Nat. Photonics **7**, 128–132 (2013).
24. A. E. Schlather, N. Large, A. S. Urban, P. Nordlander, and N. J. Halas, "Near-field mediated plexcitonic coupling and giant Rabi splitting in individual metallic dimers," Nano Lett. **13**, 3281–3286 (2013).
25. G. Zengin, G. Johansson, P. Johansson, T. J. Antosiewicz, M. Käll, and T. Shegai, "Approaching the strong coupling limit in single plasmonic nanorods interacting with J-aggregates," Sci. Rep. **3**, 3074 (2013).
26. A. Delga, J. Feist, J. Bravo-Abad, and F. J. Garcia-Vidal, "Quantum emitters near a metal nanoparticle: strong coupling and quenching," Phys. Rev. Lett. **112**, 253601 (2014).
27. T. J. Antosiewicz, S. P. Apell, and T. Shegai, "Plasmon–exciton interactions in a core–shell geometry: from enhanced absorption to strong coupling," ACS Photon. **1**, 454–463 (2014).
28. G. Zengin, M. Wersäll, S. Nilsson, T. J. Antosiewicz, M. Käll, and T. Shegai, "Realizing strong light–matter interactions between single-nanoparticle plasmons and molecular excitons at ambient conditions," Phys. Rev. Lett. **114**, 157401 (2015).
29. P. Törmä and W. L. Barnes, "Strong coupling between surface plasmon polaritons and emitters: a review," Rep. Prog. Phys. **78**, 013901 (2015).
30. J. George, S. Wang, T. Chervy, A. Canaguier-Durand, G. Schaeffer, J.-M. Lehn, J. A. Hutchison, C. Genet, and T. W. Ebbesen, "Ultra-strong coupling of molecular materials: spectroscopy and dynamics," Faraday Discuss. **178**, 281–294 (2015).
31. J. Galego, F. J. Garcia-Vidal, and J. Feist, "Cavity-induced modifications of molecular structure in the strong-coupling regime," Phys. Rev. X **5**, 041022 (2015).
32. J. Galego, F. J. Garcia-Vidal, and J. Feist, "Suppressing photochemical reactions with quantized light fields," Nat. Commun. **7**, 13841 (2016).
33. G. Zengin, T. Gschneidtner, R. Verre, L. Shao, T. J. Antosiewicz, K. Moth-Poulsen, M. Käll, and T. Shegai, "Evaluating conditions for strong coupling between nanoparticle plasmons and organic dyes using scattering and absorption spectroscopy," J. Phys. Chem. C **120**, 20588–20596 (2016).
34. D. Melnikau, R. Esteban, D. Savateeva, A. Sánchez-Iglesias, M. Grzelczak, M. K. Schmidt, L. M. Liz-Marzán, J. Aizpurua, and Y. P. Rakovich, "Rabi splitting in photoluminescence spectra of hybrid systems of gold nanorods and J-aggregates," J. Phys. Chem. Lett. **7**, 354–362 (2016).
35. J. A. Ćwik, P. Kirton, S. De Liberato, and J. Keeling, "Excitonic spectral features in strongly coupled organic polaritons," Phys. Rev. A **93**, 033840 (2016).
36. F. Herrera and F. C. Spano, "Absorption and photoluminescence in organic cavity QED," Phys. Rev. A **95**, 053867 (2017).
37. R. Sáez-Blázquez, J. Feist, A. I. Fernández-Domínguez, and F. J. García-Vidal, "Enhancing photon correlations through plasmonic strong coupling," Optica **4**, 1363–1367 (2017).
38. F. Herrera and F. C. Spano, "Dark vibronic polaritons and the spectroscopy of organic microcavities," Phys. Rev. Lett. **118**, 223601 (2017).
39. D. G. Baranov, M. Wersäll, J. Cuadra, T. J. Antosiewicz, and T. Shegai, "Novel nanostructures and materials for strong light–matter interactions," ACS Photon. **5**, 24–42 (2018).
40. F. Herrera and F. C. Spano, "Theory of nanoscale organic cavities: the essential role of vibration-photon dressed states," ACS Photon. **5**, 65–79 (2018).
41. M. A. Zeb, P. G. Kirton, and J. Keeling, "Exact states and spectra of vibrationally dressed polaritons," ACS Photon. **5**, 249–257 (2018).
42. J.-J. Greffet, P. Bouchon, G. Brucoli, and F. Marquier, "Light emission by nonequilibrium bodies: local Kirchhoff law," Phys. Rev. X **8**, 021008 (2018).
43. J. A. Hutchison, T. Schwartz, C. Genet, E. Devaux, and T. W. Ebbesen, "Modifying chemical landscapes by coupling to vacuum fields," Angew. Chem. (Int. Ed.) **51**, 1592–1596 (2012).
44. A. Canaguier-Durand, E. Devaux, J. George, Y. Pang, J. A. Hutchison, T. Schwartz, C. Genet, N. Wilhelms, J.-M. Lehn, and T. W. Ebbesen, "Thermodynamics of molecules strongly coupled to the vacuum field," Angew. Chem. (Int. Ed.) **52**, 10533–10536 (2013).
45. A. Thomas, J. George, A. Shalabney, M. Dryzhakov, S. J. Varma, J. Moran, T. Chervy, X. Zhong, E. Devaux, C. Genet, J. A. Hutchison, and T. W. Ebbesen, "Ground-state chemical reactivity under vibrational coupling to the vacuum electromagnetic field," Angew. Chem. (Int. Ed.) **55**, 11462–11466 (2016).
46. F. Herrera and F. C. Spano, "Cavity-controlled chemistry in molecular ensembles," Phys. Rev. Lett. **116**, 238301 (2016).
47. J. Flick, C. Schäfer, M. Ruggenthaler, H. Appel, and A. Rubio, "Ab-initio optimized effective potentials for real molecules in optical cavities: photon contributions to the molecular ground state," ACS Photon. **5**, 992–1005 (2017).
48. H. Deng, G. Weihs, C. Santori, J. Bloch, and Y. Yamamoto, "Condensation of semiconductor microcavity exciton polaritons," Science **298**, 199–202 (2002).
49. J. Kasprzak, M. Richard, S. Kundermann, A. Baas, P. Jeambrun, J. M. J. Keeling, F. M. Marchetti, M. H. Szymańska, R. André, J. L. Staehli, V. Savona, P. B. Littlewood, B. Deveaud, and L. S. Dang, "Bose–Einstein condensation of exciton polaritons," Nature **443**, 409–414 (2006).
50. R. Balili, V. Hartwell, D. Snoke, L. Pfeiffer, and K. West, "Bose–Einstein condensation of microcavity polaritons in a trap," Science **316**, 1007–1010 (2007).
51. G. Tosi, G. Christmann, N. Berloff, P. Tsotsis, T. Gao, Z. Hatzopoulos, P. Savvidis, and J. Baumberg, "Sculpting oscillators with light within a nonlinear quantum fluid," Nat. Phys. **8**, 190–194 (2012).
52. J. D. Plumhof, T. Stöferle, L. Mai, U. Scherf, and R. F. Mahrt, "Room-temperature Bose–Einstein condensation of cavity exciton–polaritons in a polymer," Nat. Mater. **13**, 247–252 (2014).
53. K. Daskalakis, S. Maier, R. Murray, and S. Kéna-Cohen, "Nonlinear interactions in an organic polariton condensate," Nat. Mater. **13**, 271–278 (2014).
54. D. Sanvitto and S. Kéna-Cohen, "The road towards polaritonic devices," Nat. Mater. **15**, 1061–1073 (2016).
55. C. P. Dietrich, A. Steude, L. Tropf, M. Schubert, N. M. Kronenberg, K. Ostermann, S. Höfling, and M. C. Gather, "An exciton–polariton laser based on biologically produced fluorescent protein," Sci. Adv. **2**, e1600666 (2016).
56. Y. Sun, P. Wen, Y. Yoon, G. Liu, M. Steger, L. N. Pfeiffer, K. West, D. W. Snoke, and K. A. Nelson, "Bose–Einstein condensation of long-lifetime polaritons in thermal equilibrium," Phys. Rev. Lett. **118**, 016602 (2017).

57. D. M. Coles, N. Somaschi, P. Michetti, C. Clark, P. G. Lagoudakis, P. G. Savvidis, and D. G. Lidzey, "Polariton-mediated energy transfer between organic dyes in a strongly coupled optical microcavity," Nat. Mater. **13**, 712–719 (2014).
58. X. Zhong, T. Chervy, L. Zhang, A. Thomas, J. George, C. Genet, J. A. Hutchison, and T. W. Ebbesen, "Energy transfer between spatially separated entangled molecules," Angew. Chem. (Int. Ed.) **56**, 9034–9038 (2017).
59. D. G. Lidzey, D. D. C. Bradley, T. Virgili, A. Armitage, M. S. Skolnick, and S. Walker, "Room temperature polariton emission from strongly coupled organic semiconductor microcavities," Phys. Rev. Lett. **82**, 3316–3319 (1999).
60. N. Christogiannis, N. Somaschi, P. Michetti, D. M. Coles, P. G. Savvidis, P. G. Lagoudakis, and D. G. Lidzey, "Characterizing the electroluminescence emission from a strongly coupled organic semiconductor microcavity led," Adv. Opt. Mater. **1**, 503–509 (2013).
61. M. Wersäll, J. Cuadra, T. J. Antosiewicz, S. Balci, and T. Shegai, "Observation of mode splitting in photoluminescence of individual plasmonic nanoparticles strongly coupled to molecular excitons," Nano Lett. **17**, 551–558 (2017).
62. A. Canaguier-Durand, C. Genet, A. Lambrecht, T. W. Ebbesen, and S. Reynaud, "Non-Markovian polariton dynamics in organic strong coupling," Eur. Phys. J. D **69**, 24 (2015).
63. S. Mukamel, "On the nature of intramolecular dephasing processes in polyatomic molecules," Chem. Phys. **31**, 327–333 (1978).
64. J. del Pino, F. A. Schröder, A. W. Chin, J. Feist, and F. J. García-Vidal, "Tensor network simulation of non-Markovian dynamics in organic polaritons," arXiv:1804.04511 (2018).
65. B. Li, A. E. Johnson, S. Mukamel, and A. B. Myers, "The Brownian oscillator model for solvation effects in spontaneous light emission and their relationship to electron transfer," J. Am. Chem. Soc. **116**, 11039–11047 (1994).
66. J. Tomasi, B. Mennucci, and R. Cammi, "Quantum mechanical continuum solvation models," Chem. Rev. **105**, 2999–3094 (2005).
67. H.-P. Breuer and F. Petruccione, *The Theory of Open Quantum Systems* (Oxford University, 2003).
68. T.-S. Yang, P. Vöhringer, D. C. Arnett, and N. F. Scherer, "The solvent spectral density and vibrational multimode approach to optical dephasing: two-pulse photon echo response," J. Chem. Phys. **103**, 8346–8359 (1995).
69. C. Roy and S. Hughes, "Influence of electron–acoustic-phonon scattering on intensity power broadening in a coherently driven quantum-dot–cavity system," Phys. Rev. X **1**, 021009 (2011).
70. L. A. Pachón and P. Brumer, "Direct experimental determination of spectral densities of molecular complexes," J. Chem. Phys. **141**, 174102 (2014).
71. K. Roy-Choudhury and S. Hughes, "Spontaneous emission from a quantum dot in a structured photonic reservoir: phonon-mediated breakdown of Fermi's golden rule," Optica **2**, 434–437 (2015).
72. J. del Pino, J. Feist, and F. J. Garcia-Vidal, "Quantum theory of collective strong coupling of molecular vibrations with a microcavity mode," New J. Phys. **17**, 053040 (2015).
73. M. M. Toutounji and G. J. Small, "The underdamped Brownian oscillator model with Ohmic dissipation: applicability to low-temperature optical spectra," J. Chem. Phys. **117**, 3848–3855 (2002).
74. J. Roden, W. T. Strunz, K. B. Whaley, and A. Eisfeld, "Accounting for intra-molecular vibrational modes in open quantum system description of molecular systems," J. Chem. Phys. **137**, 204110 (2012).
75. C. Kreisbeck and T. Kramer, "Long-lived electronic coherence in dissipative exciton dynamics of light-harvesting complexes," J. Phys. Chem. Lett. **3**, 2828–2833 (2012).
76. A. Kell, X. Feng, M. Reppert, and R. Jankowiak, "On the shape of the phonon spectral density in photosynthetic complexes," J. Phys. Chem. B **117**, 7317–7323 (2013).
77. V. M. Agranovich, M. Litinskaia, and D. G. Lidzey, "Cavity polaritons in microcavities containing disordered organic semiconductors," Phys. Rev. B **67**, 085311 (2003).
78. R. Sáez-Blázquez, J. Feist, A. I. Fernández-Domnguez, and F. J. Garca-Vidal, "Organic polaritons enable local vibrations to drive long-range energy transfer," Phys. Rev. B **97**, 241407 (2018).
79. R. F. Ribeiro, L. A. Martínez-Martínez, M. Du, J. Campos-Gonzalez-Angulo, and J. Yuen-Zhou, "Polariton chemistry: controlling molecular dynamics with optical cavities," Chem. Sci. **9**, 6325–6339 (2018).
80. M. Du, L. A. Martínez-Martínez, R. F. Ribeiro, Z. Hu, V. M. Menon, and J. Yuen-Zhou, "Theory for polariton-assisted remote energy transfer," Chem. Sci. **9**, 6659–6669 (2018).
81. R. Chikkaraddy, B. de Nijs, F. Benz, S. J. Barrow, O. A. Scherman, E. Rosta, A. Demetriadou, P. Fox, O. Hess, and J. J. Baumberg, "Single-molecule strong coupling at room temperature in plasmonic nanocavities," Nature **535**, 127–130 (2016).
82. T. Virgili, D. Coles, A. M. Adawi, C. Clark, P. Michetti, S. K. Rajendran, D. Brida, D. Polli, G. Cerullo, and D. G. Lidzey, "Ultrafast polariton relaxation dynamics in an organic semiconductor microcavity," Phys. Rev. B **83**, 245309 (2011).
83. T. Schwartz, J. A. Hutchison, J. Léonard, C. Genet, S. Haacke, and T. W. Ebbesen, "Polariton dynamics under strong light–molecule coupling," Chem. Phys. Chem. **14**, 125–131 (2013).
84. S. Wang, T. Chervy, J. George, J. A. Hutchison, C. Genet, and T. W. Ebbesen, "Quantum yield of polariton emission from hybrid light–matter states," J. Phys. Chem. Lett. **5**, 1433–1439 (2014).